Structure-Preserving Discretization of a Coupled Heat-Wave System, as Interconnected Port-Hamiltonian Systems

Ghislain Haine(✉) and Denis Matignon

ISAE-SUPAERO, Université de Toulouse, Toulouse, France
{ghislain.haine,denis.matignon}@isae.fr

Abstract. The heat-wave system is recast as the coupling of port-Hamiltonian subsystems (pHs), and discretized in a structure-preserving way by the Partitioned Finite Element Method (PFEM) [10,11]. Then, depending on the geometric configuration of the two domains, different asymptotic behaviours of the energy of the coupled system can be recovered at the numerical level, assessing the validity of the theoretical results of [22].

Keywords: Port-Hamiltonian Systems · Partitioned finite element method · Long time asymptotics

1 Introduction and Main Results

Multi-physical systems arise in many areas of science, and high-fidelity simulations are often needed to reduce the number of real-life experiments, hence the cost of optimal design in industry. Such problems can be encountered for instance in aeronautics [12], in chemistry [1] and so on [20]. A first difficulty consists in finding an admissible way to model each physical subsystem of the experiment, with a precise identification of negligible phenomena, as well as feasible controls and available measurements. The second difficulty lies in the coupling of the subsystems altogether to build the final system to simulate. And the last difficulties are obviously the construction of appropriate discretization schemes and the simulations themselves.

Port-Hamiltonian systems (pHs) have been extended to infinite-dimensional setting in [21] two decades ago, allowing to tackle Partial Differential Equations (PDE), and especially those appearing in physics. One of the major force of the port-Hamiltonian approach lies in its ease of use for coupling, since the resulting system remains a pHs [13]. Another strength is its versatility with respect to the

This work has been performed in the frame of the Collaborative Research DFG and ANR project INFIDHEM, entitled *Interconnected Infinite-Dimensional systems for Heterogeneous Media*, n° ANR-16-CE92-0028. Further information is available at https://websites.isae-supaero.fr/infidhem/the-project/.

F. Nielsen and F. Barbaresco (Eds.): GSI 2021, LNCS 12829, pp. 191–199, 2021.
https://doi.org/10.1007/978-3-030-80209-7_22

conditions of experiment: on the one hand, axioms of (classical) physics are used to derive an algebraic structure, namely the Stokes-Dirac structure, and on the other hand, physical laws, state equations, and definitions of physical variables close the system (in the algebraic sense).

This formalism seems very appropriate also for structured computer codes dedicated to efficient simulation. Indeed, each subsystem of the general experiment can be separately discretized before the interconnection: provided that the discretization is structured-preserving, meaning that it leads to a finite-dimensional pHs, the final simulation will enjoy the aforementioned advantages. Furthermore, if each subsystem is also well-structured, meaning that it keeps the separation of axioms and laws, the final simulation codes should be easy to enrich with more and more models. This is the purpose of the discretization scheme known as the Partitioned Finite Element Method (PFEM) [11], which can be seen as an adaptation of the well-known, well-proved, and robust Mixed Finite Element Method (MFEM) [5], not to mention that most, if not all, scientific programming languages already propose finite element libraries [9]. PFEM proves to be very well-adapted to discretized pHs and shows an ever-growing range of applications [6,7,17,19]. Nevertheless, only a few of them tackle and test the interconnection problem [8].

The goal of this work is to provide an application of PFEM, together with numerical simulations, for a simplified and linearised system of fluid-structure interaction (FSI), for which long-time behaviour is known [2,22]. Since PFEM aims at mimicking the pHs structure at the discrete level, hence the power balance satisfied by the *energy* of the system, a good approximation of the long-time behaviour provided in [22] is expected.

1.1 A Simplified and Linearised Fluid-Structure Model

Let $\Omega \subset \mathbb{R}^n$ be a bounded domain with a $\mathcal{C}^2$ boundary $\Gamma := \partial\Omega$. Let Ω_1 be a subdomain of Ω and $\Omega_2 := \Omega \setminus \overline{\Omega_1}$. Denote Γ_{int} the interface, $\Gamma_j := \partial\Omega_j \setminus \overline{\Gamma_{\text{int}}}$ $(j = 1, 2)$, and $\boldsymbol{n}_j$ the unit outward normal vector to Ω_j. Note that $\Gamma = \overline{\Gamma_1 \cup \Gamma_2}$.

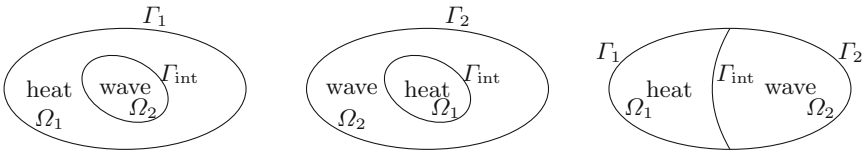

Fig. 1. Different geometrical configurations

We are interested in the structure-preserving discretisation of the following system, $\forall t > 0$:

$$\begin{cases} \partial_t T(t,\boldsymbol{x}) - \Delta T(t,\boldsymbol{x}) = 0, \boldsymbol{x} \in \Omega_1, \\ T(t,\boldsymbol{x}) = 0, \boldsymbol{x} \in \Gamma_1, \end{cases} \quad \begin{cases} \partial_{tt} w(t,\boldsymbol{x}) - \Delta w(t,\boldsymbol{x}) = 0, \boldsymbol{x} \in \Omega_2, \\ w(t,\boldsymbol{x}) = 0, \boldsymbol{x} \in \Gamma_2, \end{cases} \tag{1}$$

together with transmission conditions across the boundary Γ_{int}:

$$T(t,\boldsymbol{x}) = \partial_t w(t,\boldsymbol{x}), \quad \text{and} \quad \partial_{\boldsymbol{n}_1} T(t,\boldsymbol{x}) = -\partial_{\boldsymbol{n}_2} w(t,\boldsymbol{x}), \quad \forall\, t>0,\, \boldsymbol{x}\in\Gamma_{\text{int}}, \tag{2}$$

and initial data $T(0,\boldsymbol{x}) = T_0(\boldsymbol{x}), \forall \boldsymbol{x}\in\Omega_1$, and $w(0,\boldsymbol{x}) = w_0(\boldsymbol{x})$, $\partial_t w(0,\boldsymbol{x}) = w_1(\boldsymbol{x}), \forall \boldsymbol{x}\in\Omega_2$.

From [22, Thm. 1], it is known that (1)–(2) is well-posed in the *finite energy space* $\mathcal{X} := L^2(\Omega_1)\times H^1_{\Gamma_2}(\Omega_2)\times L^2(\Omega_2)$, endowed with the following norm:

$$\|\boldsymbol{u}\|^2_{\mathcal{X}} := \|u_1\|^2_{L^2(\Omega_1)} + \|u_2\|^2_{L^2(\Omega_2)} + \|\boldsymbol{\nabla}\,(u_2)\|^2_{(L^2(\Omega_2))^n} + \|u_3\|^2_{L^2(\Omega_1)}\,. \tag{3}$$

The semi-norm $|\boldsymbol{u}|^2_{\mathcal{X}} := \|u_1\|^2_{L^2(\Omega_1)} + \|\boldsymbol{\nabla}\,(u_2)\|^2_{(L^2(\Omega_2))^n} + \|u_3\|^2_{L^2(\Omega_1)}$ is a norm on $\mathcal{X}$, equivalent to (3), when Γ_2 has strictly positive measure.

In [22, Thm. 11 & 13], the asymptotic behaviours of these (semi-)norms have been proved, depending on the geometry of Ω (see Fig. 1).

1.2 Main Contributions and Organisation of the Paper

As a major result, we provide a numerical method able to mimick the expected time behaviour in the different geometrical configurations of Fig. 1.

In Sect. 2, the heat and wave PDEs are recast as port-Hamiltonian systems (pHs). In Sect. 3, the Partitioned Finite Element Method (PFEM) is recalled and applied to the coupled system. In Sect. 4, numerical results are provided and compared with the theoretical results of [22].

2 Port-Hamiltonian Formalism

The physical models are recast as port-Hamiltonian systems. However, all physical parameters are taken equal to 1, to stick to system (1)–(2) studied in [22].

2.1 The Fluid Model

The simplified linearised model used for the fluid is the heat equation. The chosen representation corresponds to the *Lyapunov* case already presented in [16,18], with Hamiltonian $\mathcal{H}_1(t) = \frac{1}{2}\int_{\Omega_1} T^2(t,\boldsymbol{x})\,\mathrm{d}\boldsymbol{x}$, where T denotes the temperature. Denoting $\boldsymbol{J}_Q$ the heat flux, the port-Hamiltonian system reads:

$$\begin{pmatrix} \partial_t T \\ -\boldsymbol{\nabla} T \end{pmatrix} = \begin{bmatrix} 0 & -\mathrm{div} \\ -\boldsymbol{\nabla} & 0 \end{bmatrix} \begin{pmatrix} T \\ \boldsymbol{J}_Q \end{pmatrix}, \tag{4}$$

together with boundary ports:

$$\boldsymbol{\nabla} T(t,\boldsymbol{x})\cdot\boldsymbol{n}_1(\boldsymbol{x}) = u_1(t,\boldsymbol{x}), \quad y_1(t,\boldsymbol{x}) = T(t,\boldsymbol{x}), \quad \forall\, t>0,\, \boldsymbol{x}\in\Gamma_{\text{int}}, \tag{5}$$

$$T(t,\boldsymbol{x}) = 0, \quad y_T(t,\boldsymbol{x}) = \boldsymbol{\nabla} T(t,\boldsymbol{x})\cdot\boldsymbol{n}_1(\boldsymbol{x}), \quad \forall\, t>0,\, \boldsymbol{x}\in\Gamma_1. \tag{6}$$

To close the system, Fourier's law has been used as constitutive relation: $\boldsymbol{J}_Q = -\boldsymbol{\nabla} T$. The power-balance of the lossy heat subsystem classically reads:

$$\frac{\mathrm{d}}{\mathrm{d}t}\mathcal{H}_1 = -\int_{\Omega_1} |\boldsymbol{\nabla} T|^2 + \langle u_1, y_1\rangle_{H^{-\frac{1}{2}}(\Gamma_{\text{int}}),H^{\frac{1}{2}}(\Gamma_{\text{int}})}\,. \tag{7}$$

2.2 The Structure Model

The structure model is the wave equation, a hyperbolic equation widely studied as a pHs (see *e.g.* [19]). The Hamiltonian is the sum of the kinetic and potential energies, $\mathcal{H}_2(t) = \frac{1}{2}\int_{\Omega_2} (\partial_t w(t,\boldsymbol{x}))^2 + |\boldsymbol{\nabla} w(t,\boldsymbol{x})|^2 \ \mathrm{d}\boldsymbol{x}$, w being the deflection and $\partial_t w$ its velocity. The port-Hamiltonian system reads:

$$\begin{pmatrix} \partial_t(\partial_t w) \\ \partial_t(\boldsymbol{\nabla} w) \end{pmatrix} = \begin{bmatrix} 0 & \mathrm{div} \\ \boldsymbol{\nabla} & 0 \end{bmatrix} \begin{pmatrix} \partial_t w \\ \boldsymbol{\nabla} w \end{pmatrix}, \tag{8}$$

together with boundary ports:

$$\partial_t w(t,\boldsymbol{x}) = u_2(t,\boldsymbol{x}), \quad y_2(t,\boldsymbol{x}) = \boldsymbol{\nabla} w(t,\boldsymbol{x}) \cdot \boldsymbol{n}_2(\boldsymbol{x}), \quad \forall\, t > 0,\, \boldsymbol{x} \in \Gamma_{\mathrm{int}}, \tag{9}$$

$$\partial_t w(t,\boldsymbol{x}) = 0, \quad y_w(t,\boldsymbol{x}) = \boldsymbol{\nabla} w(t,\boldsymbol{x}) \cdot \boldsymbol{n}_2(\boldsymbol{x}), \quad \forall\, t > 0,\, \boldsymbol{x} \in \Gamma_2. \tag{10}$$

The power-balance of the lossless wave subsystem is:

$$\frac{\mathrm{d}}{\mathrm{d}t}\mathcal{H}_2 = \langle y_2, u_2 \rangle_{H^{-\frac{1}{2}}(\Gamma_{\mathrm{int}}), H^{\frac{1}{2}}(\Gamma_{\mathrm{int}})}. \tag{11}$$

2.3 The Coupled System

First note that the homogeneous boundary conditions of (1) have already been taken into account in (6) and (10). The coupling is then obtained by a *gyrator* interconnection of the boundary ports on Γ_{int}, meaning that the input of one system is fully determined by the output of the other one, namely:

$$u_1(t,\boldsymbol{x}) = -y_2(t,\boldsymbol{x}), \qquad u_2(t,\boldsymbol{x}) = y_1(t,\boldsymbol{x}), \quad \forall\, t > 0,\, \boldsymbol{x} \in \Gamma_{\mathrm{int}}. \tag{12}$$

As a consequence, the closed coupled system proves dissipative, since the power balance for the global Hamiltonian, $\mathcal{H} = \mathcal{H}_1 + \mathcal{H}_2 := \frac{1}{2}\left|(T, w, \partial_t w)\right|^2_{\mathcal{X}}$, reads:

$$\frac{\mathrm{d}}{\mathrm{d}t}\mathcal{H} = -\int_{\Omega_1} |\boldsymbol{\nabla} T|^2. \tag{13}$$

3 The Partitioned Finite Element Method

The main idea of PFEM, as in the mixed finite element method, is to integrate by parts only one line of the weak formulation of the system. For our purpose, the choice of which line is to be integrated by parts is dictated by the desired boundary control, see [11] and references therein for more details.

The method leads to a finite-dimensional pHs, which enjoys a discrete power balance, mimicking the continuous one: it is thus structure-preserving. The interconnection of each subsystem is then made using the pHs structure, ensuring an accurate discrete power balance for the coupled system.

3.1 For the Fluid

The heat equation with Hamiltonian $\mathcal{H}_1$ has already been addressed in [17]. The difficulty lies in the mixed Dirichlet–Neumann boundary conditions. Here, following [8], we choose the Lagrange multiplier approach. Let $\boldsymbol{\psi}^1$, φ^1 and ξ^1 be smooth test functions (resp. vectorial, scalar, and scalar at the boundary). Using γ_0 the Dirichlet trace, the weak form of (4)–(5)–(6) reads, after integration by parts of the first line and taking Fourier's law into account in the second:

$$\begin{cases} \int_\Omega \partial_t T\, \varphi^1 = \int_\Omega \boldsymbol{J}_Q \cdot \boldsymbol{\nabla}(\varphi^1) - \int_{\Gamma_1} y_T\, \gamma_0(\varphi^1) - \int_{\Gamma_{\text{int}}} u_1\, \gamma_0(\varphi^1), \\ \int_\Omega \boldsymbol{J}_Q \cdot \boldsymbol{\psi}^1 = -\int_\Omega \boldsymbol{\nabla}(T) \cdot \boldsymbol{\psi}^1, \\ \int_{\Gamma_1} \gamma_0(T)\, \xi^1 = 0, \\ \int_{\Gamma_{\text{int}}} y_1\, \xi^1 = \int_{\Gamma_{\text{int}}} \gamma_0(T)\, \xi^1. \end{cases}$$

The output y_T is the Lagrange multiplier of the Dirichlet constraint on 3rd line.

Let $(\boldsymbol{\psi}_i^1)_{1\le i\le N_Q}$, $(\varphi_j^1)_{1\le j\le N_T}$, $(\xi_k^1)_{1\le k\le N_{\Gamma_1}}$ and $(\xi_k^{\text{int}})_{1\le k\le N_{\Gamma_{\text{int}}}}$ be finite elements (FE) bases. Note that boundary functions ξ^1 have been divided in two distinct families, on Γ_1 and Γ_{int}. Approximating each quantity in the appropriate basis leads to a port-Hamiltonian Differential Algebraic Equation (pHDAE) [4,15]:

$$\begin{bmatrix} M_T & 0 & 0 & 0 \\ 0 & M_Q & 0 & 0 \\ 0 & 0 & M_1 & 0 \\ 0 & 0 & 0 & M_{\text{int}} \end{bmatrix} \begin{pmatrix} \dot{\underline{T}} \\ \underline{J_Q} \\ \underline{0} \\ -\underline{y_1} \end{pmatrix} = \begin{bmatrix} 0 & D_1 & B_1 & B_{\text{int}} \\ -D_1^\top & 0 & 0 & 0 \\ -B_1^\top & 0 & 0 & 0 \\ -B_{\text{int}}^\top & 0 & 0 & 0 \end{bmatrix} \begin{pmatrix} \underline{T} \\ \underline{J_Q} \\ \underline{y_T} \\ \underline{u_1} \end{pmatrix}, \tag{14}$$

where $M_\star$ is the mass matrix of the FE basis corresponding to $\star$, $\underline{\star}$ is the column vector collecting the coefficients of the approximation of $\star$ in its FE basis, and:

$$(D_1)_{j,i} = \int_{\Omega_1} \boldsymbol{\psi}_i^1 \cdot \boldsymbol{\nabla}(\varphi_j^1) \in \mathbb{R}^{N_T \times N_Q}, \quad (B_\star)_{j,k} = -\int_{\Gamma_\star} \xi_k^\star\, \gamma_0(\varphi_j^1) \in \mathbb{R}^{N_T \times N_{\Gamma_\star}}.$$

Defining the discrete Hamiltonian $\mathcal{H}_1^d$ as the evaluation of $\mathcal{H}_1$ on $T^d := \sum_{j=1}^{N_T} T_j \varphi_j^1$, one gets $\mathcal{H}_1^d(t) = \frac{1}{2}\underline{T}^\top M_T \underline{T}$. Thanks to the structure of (14), it satisfies a perfectly mimicking discrete counterpart of (7):

$$\frac{\mathrm{d}}{\mathrm{d}t}\mathcal{H}_1^d = -\underline{J_Q}^\top M_Q \underline{J_Q} + \underline{u_1}^\top M_{\text{int}} \underline{y_1}. \tag{15}$$

3.2 For the Structure

The wave equation, studied in *e.g.* [19], does not present difficulty here, since only Dirichlet boundary conditions are considered. One can integrate by parts the second line of the weak form of (8)–(9)–(10) and project on FE bases $(\boldsymbol{\psi}_i^2)_{1\le i\le N_q}$, $(\varphi_j^2)_{1\le j\le N_p}$, $(\xi_k^2)_{1\le k\le N_{\Gamma_2}}$ and $(\xi_k^{\text{int}})_{1\le k\le N_{\Gamma_{\text{int}}}}$, where q-type quantities are related to stress and strain ($\boldsymbol{\alpha}_q := \boldsymbol{\nabla}(w)$) and p-type quantities to linear

momentum and velocity ($\alpha_p := \partial_t w$). The finite-dimensional pHs then reads:

$$\begin{bmatrix} M_p & 0 & 0 & 0 \\ 0 & M_q & 0 & 0 \\ 0 & 0 & M_2 & 0 \\ 0 & 0 & 0 & M_{\text{int}} \end{bmatrix} \begin{pmatrix} \dot{\underline{\alpha_p}} \\ \dot{\underline{\boldsymbol{\alpha}_q}} \\ -\underline{y_q} \\ -\underline{y_2} \end{pmatrix} = \begin{bmatrix} 0 & D_2 & 0 & 0 \\ -D_2^\top & 0 & B_2 & B_{\text{int}} \\ 0 & -B_2^\top & 0 & 0 \\ 0 & -B_{\text{int}}^\top & 0 & 0 \end{bmatrix} \begin{pmatrix} \underline{\alpha_p} \\ \underline{\boldsymbol{\alpha}_q} \\ \underline{0} \\ \underline{u_2} \end{pmatrix}, \tag{16}$$

$$\text{with } (D_2)_{j,i} = \int_{\Omega_2} \operatorname{div}(\boldsymbol{\psi}_j^2)\, \varphi_i^2 \in \mathbb{R}^{N_p \times N_q}, \quad (B_\star)_{j,k} = -\int_{\Gamma_\star} \xi_k^\star\, \boldsymbol{\phi}_j^2 \cdot \boldsymbol{n}_2 \in \mathbb{R}^{N_q \times N_{\Gamma_\star}}.$$

Defining the discrete Hamiltonian $\mathcal{H}_2^d(t) = \frac{1}{2}\left(\underline{\alpha_p}^\top M_p \underline{\alpha_p} + \underline{\boldsymbol{\alpha}_q}^\top M_q \underline{\boldsymbol{\alpha}_q}\right)$, thanks to the structure of (16), one easily gets the discrete counterpart of (11):

$$\frac{\mathrm{d}}{\mathrm{d}t}\mathcal{H}_2^d = \underline{u_2}^\top M_{\text{int}} \underline{y_2}. \tag{17}$$

3.3 Coupling by Gyrator Interconnection

The gyrator interconnection (12) is now imposed weakly, at the discrete level: for all ξ^{int}, smooth boundary test functions on Γ_{int}:

$$\int_{\Gamma_{\text{int}}} \xi^{\text{int}} u_1 = -\int_{\Gamma_{\text{int}}} \xi^{\text{int}} y_2, \quad \int_{\Gamma_{\text{int}}} \xi^{\text{int}} u_2 = \int_{\Gamma_{\text{int}}} \xi^{\text{int}} y_1.$$

After projection on the FE basis $(\xi_k^{\text{int}})_{1 \le k \le N_{\Gamma_{\text{int}}}}$, this becomes:

$$M_{\text{int}} \underline{u_1} = -M_{\text{int}} \underline{y_2}, \quad M_{\text{int}} \underline{u_2} = M_{\text{int}} \underline{y_1}. \tag{18}$$

In Sect. 4, the interconnection matrix $C := B_1 M_{\text{int}}^{-1} B_2^\top$ (and its transpose) is used. However, the inverse M_{int}^{-1} appearing is not a drawback, since only the interface mass matrix is involved, which is of very small size.

The total discrete Hamiltonian $\mathcal{H}^d = \mathcal{H}_1^d + \mathcal{H}_2^d$ then satisfies thanks to (18):

$$\frac{\mathrm{d}}{\mathrm{d}t}\mathcal{H}^d = -\underline{J_Q}^\top M_Q \underline{J_Q} - \underline{y_2}^\top M_{\text{int}} \underline{y_1} + \underline{y_1}^\top M_{\text{int}} \underline{y_2} = -\underline{J_Q}^\top M_Q \underline{J_Q},$$

which perfectly mimics (13) with no approximation (compare with [3,14]): hence, PFEM also proves to be a reliable structure-preserving method for coupled pHs.

4 Numerical Simulations

In order to test numerically the behaviours proved in [22], two geometries are chosen. Switching the domains Ω_1 and Ω_2, four cases are covered. These geometries are given in Fig. 2. The time integration is performed by IDA SUNDIALS (BDF adaptative scheme) *via* `assimulo`. Moreover, $\mathbb{P}^1$ Lagrange elements of order 1 (both distributed and at the boundary) have been used for scalar fields, while RT1 Raviart-Thomas elements of order 1 have been used for vector fields.

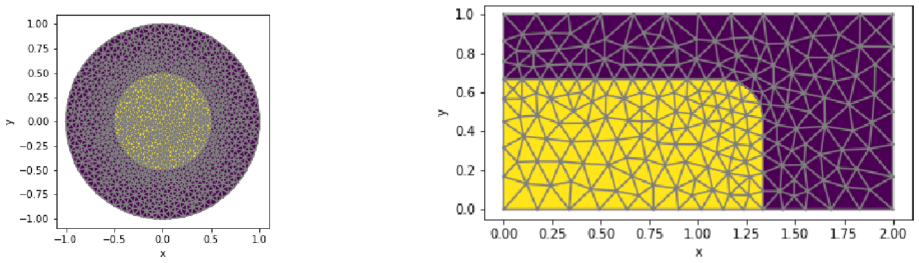

Fig. 2. The colors define the subdomains Ω_1 and Ω_2. On the left, either Γ_1 or Γ_2 is empty. On the right, either Ω_1 is the L-shape subdomain and the geometric optic condition (GCC) is satisfied in Ω, or Ω_1 is the rectangle and the GCC fails.

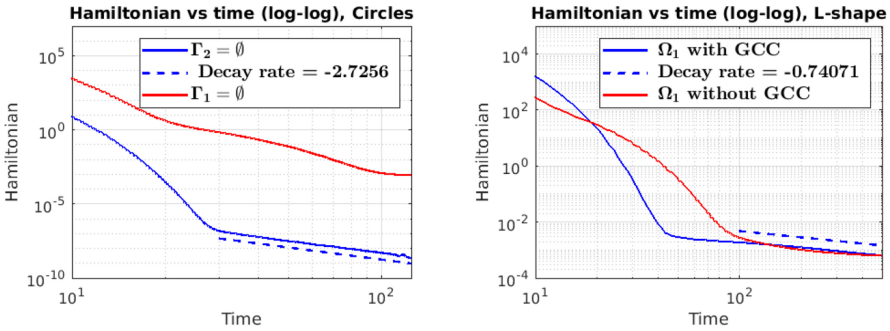

Fig. 3. On the left, the "circles" cases. On the right, the "L-shape" cases.

On the one hand, when $\Gamma_2 = \emptyset$ or when the GCC is satisfied by Ω_1, [22, Thm. 11] asserts a polynomial decay, of rate at least $-1/3$. One can appreciate the blue curves on both plots of Fig. 3, showing this polynomial decay (dashed blue lines) in the long time range. On the other hand, when $\Gamma_1 = \emptyset$ or when the GCC fails, [22, Thm. 13, Rem. 20 & 22] assert that the best decay that could be expected is logarithmic. This is indeed the asymptotic behaviour of the red curves on both plots of Fig. 3.

Note that even in the case of a very coarse mesh (see the "L-shape" case on Fig. 2) and the apparent loss of precision on the right plot of Fig. 3, PFEM still captures the underlying structure, hence the expected decays.

5 Conclusion

PFEM also proves efficient for the structure-preserving simulation of coupled pHs, and long time (polynomial) behaviour can be recovered in many cases.

Further works concern more realistic fluid-structure interactions, *i.e.* nonlinear ones, also moving body, hence moving interface, applied *e.g.* to piston dynamics.

References

1. Altmann, R., Schulze, P.: A port-Hamiltonian formulation of the Navier-Stokes equations for reactive flows. Syst. Control Lett. **100**, 51–55 (2017)
2. Avalos, G., Lasiecka, I., Triggiani, R.: Heat-wave interaction in 2–3 dimensions: optimal rational decay rate. J. Math. Anal. Appl. **437**, 782–815 (2016)
3. Bauer, W., Gay-Balmaz, F.: Towards a geometric variational discretization of compressible fluids: the rotating shallow water equations. J. Comput. Dyn. **6**(1), 1–37 (2019)
4. Beattie, C., Mehrmann, V., Xu, H., Zwart, H.: Linear port-Hamiltonian descriptor systems. Math. Control Signals Syst. **30**(4), 1–27 (2018). https://doi.org/10.1007/s00498-018-0223-3
5. Boffi, D., Brezzi, F., Fortin, M.: Mixed Finite Element Methods and Applications. Springer Series in Computational Mathematics, vol. 44. Springer, Heidelberg (2013). https://doi.org/10.1007/978-3-642-36519-5
6. Brugnoli, A., Alazard, D., Pommier-Budinger, V., Matignon, D.: Port-Hamiltonian formulation and symplectic discretization of plate models Part I: Mindlin model for thick plates. Appl. Math. Model. **75**, 940–960 (2019)
7. Brugnoli, A., Alazard, D., Pommier-Budinger, V., Matignon, D.: Port-Hamiltonian formulation and symplectic discretization of plate models Part II: Kirchhoff model for thin plates. Appl. Math. Model. **75**, 961–981 (2019)
8. Brugnoli, A., Cardoso-Ribeiro, F.L., Haine, G., Kotyczka, P.: Partitioned finite element method for power-preserving structured discretization with mixed boundary conditions. IFAC-PapersOnLine **53**(2), 7647–7652 (2020)
9. Brugnoli, A., Haine, G., Serhani, A., and Vasseur, X.: Numerical approximation of port-Hamiltonian systems for hyperbolic or parabolic PDEs with boundary control. J. Appl. Math. Phys. **9**(6), 1278–1321 (2021). Supplementary material https://doi.org/10.5281/zenodo.3938600
10. Cardoso-Ribeiro, F.L., Matignon, D., Lefèvre, L.: A structure-preserving Partitioned Finite Element Method for the 2D wave equation. IFAC-PapersOnLine **51**(3), 119–124 (2018)
11. Cardoso-Ribeiro, F.L., Matignon, D., Lefèvre, L.: A partitioned finite element method for power-preserving discretization of open systems of conservation laws. IMA J. Math. Control Inf. (2020). https://doi.org/10.1093/imamci/dnaa038
12. Cardoso-Ribeiro, F.L., Matignon, D., Pommier-Budinger, V.: Port-Hamiltonian model of two-dimensional shallow water equations in moving containers. IMA J. Math. Control Inf. **37**, 1348–1366 (2020)
13. Cervera, J., van der Schaft, A.J., Baños, A.: Interconnection of port-Hamiltonian systems and composition of Dirac structures. Automatica **43**(2), 212–225 (2007)
14. Egger, H.: Structure-preserving approximation of dissipative evolution problems. Numerische Mathematik **143**(1), 85–106 (2019)
15. Mehrmann, V., Morandin, R.: Structure-preserving discretization for port-Hamiltonian descriptor systems. In: IEEE 58th Conference on Decision and Control (CDC), Nice, France, pp. 6863–6868. IEEE (2019)
16. Serhani, A., Haine, G., Matignon, D.: Anisotropic heterogeneous n-D heat equation with boundary control and observation: I. Modeling as port-Hamiltonian system. FAC-PapersOnLine **52**(7), 51–56 (2019)
17. Serhani, A., Haine, G., Matignon, D.: Anisotropic heterogeneous n-D heat equation with boundary control and observation: II. Structure-preserving discretization. IFAC-PapersOnLine **52**(7), 57–62 (2019)

18. Serhani, A., Matignon, D., Haine, G.: A partitioned finite element method for the structure-preserving discretization of damped infinite-dimensional port-Hamiltonian systems with boundary control. In: Nielsen, F., Barbaresco, F. (eds.) GSI 2019. LNCS, vol. 11712, pp. 549–558. Springer, Cham (2019). https://doi.org/10.1007/978-3-030-26980-7_57
19. Serhani, A., Matignon, D., Haine, G.: Partitioned Finite Element Method for port-Hamiltonian systems with boundary damping: anisotropic heterogeneous 2-D wave equations. IFAC-PapersOnLine **52**(2), 96–101 (2019)
20. van der Schaft, A., Jeltsema, D.: Port-Hamiltonian systems theory: an introductory overview. Found. Trends Syst. Control **1**(2–3), 173–378 (2014)
21. van der Schaft, A.J., Maschke, B.: Hamiltonian formulation of distributed-parameter systems with boundary energy flow. J. Geom. Phys. **42**(1–2), 166–194 (2002)
22. Zhang, X., Enrique, Z.: Long-time behavior of a coupled heat-wave system arising in fluid-structure interaction. Arch. Rat. Mech. Anal. **184**, 49–120 (2007)